Soft Matter

RSC Publishing

PAPER

View Article Online
View Journal | View Issue

Cite this: *Soft Matter*, 2013, **9**, 4705

In vitro wrinkle formation *via* shape memory dynamically aligns adherent cells†

Pine Yang,‡ Richard M. Baker,‡ James H. Henderson* and Patrick T. Mather*

Surface wrinkling of materials offers a simple yet elegant approach to fabricating cell culture substrates with highly ordered topographies for investigating cell mechanobiology. In this study we present a tunable shape memory polymer (SMP) bilayer system that is programmed to form, under cell compatible conditions, wrinkles with feature sizes on the micron and sub-micron length scale. We found that with increasing deformation fixed into the SMP substrate, wrinkled topographies with increasing amplitudes, decreasing wavelengths, and increasing degree of wrinkle orientation were achieved. Analysis of the cellular response to previously wrinkled (static) substrates revealed that cell nuclear alignment increased as SMP deformation increased. Analysis of the cellular response to an actively wrinkling substrate demonstrated that cell alignment can be controlled by triggering wrinkle formation. These findings demonstrate that the amount of deformation fixed (and later recovered) in an SMP bilayer system can be used to control the resulting wrinkle characteristics and cell mechanobiological response. The tailored and dynamic substrate functionality provided by this approach is expected to enable new investigation and understanding of cell mechanobiology.

Received 3rd January 2013
Accepted 6th March 2013

DOI: 10.1039/c3sm00024a

www.rsc.org/softmatter

Introduction

Ordered patterns with feature sizes on the micron and sub-micron scale play an important role in cell mechanobiology *in vivo*. Cells actively probe and respond to their microenvironment, and the extracellular matrix (ECM) contains proteins with feature sizes in this range that can direct cell function. Cell–matrix interactions have been found to be critical to many biological processes, including angiogenesis,[1] embryogenesis,[2] and tumorigenesis.[3] While it is known that cell–matrix interactions play a role in biological development, the fundamental mechanisms underlying the cell response largely remain unclear, and technologies exploiting the interactions have remained elusive.

To better understand how cell–matrix interactions direct cell behavior, synthetic substrates of defined topographies on the micro- and nano-scale have been developed and applied *in vitro*. Topographies have included nanofibers,[4] nanogratings,[5,6] and nanopillars and nanopits.[7] Studies employing such substrates have shown that cell alignment, migration, proliferation, and cell lineage specification are affected by topography.[5,6,8,9] The structure and size of the topographical features as well as the cell species and cell type determine the nature and extent of the cell response.[10]

Surface wrinkling offers an elegant alternative to direct molding of surface topographies for the purpose of controlled cell–material interaction. Surface buckling, or wrinkling, is a natural phenomenon that occurs in daily life. In a bilayer system consisting of a thick compliant substrate and a thin rigid coating undergoing compression, whether by differential thermal contraction,[11,12] externally applied compressive force,[13] or differential swelling or shrinkage,[14–16] the rigid coating buckles to yield distinct wrinkling patterns ranging from homogeneous[17] to hierarchical[18–21] wrinkles, one-dimensional ripple pattern[22] to two-dimensional herringbone[23,24] and more complex patterns.[12,25,26] The Burdick lab has reported interesting studies on swelling-induced wrinkles on hydrogels and their interactions with stem cells.[27,28] Models describing the mechanics of wrinkle formation provide predictions of the amplitude and wavelength within the frameworks of small[29,30] and large[31] strain deformation, giving promise for the control of such features to the extent that compressive strain can be manipulated. For small deformations, wrinkle formation is well modelled by minimizing the total elastic energy[29,32] in a uniaxial bilayer wrinkle system whose wavelength and amplitude A are given as follows:

$$\lambda = 2\pi h_f \left(\frac{\overline{E}_f}{3\overline{E}_s}\right)^{\frac{1}{3}}$$

Syracuse Biomaterials Institute and Department of Biomedical and Chemical Engineering, Syracuse University, Syracuse, NY, USA. E-mail: ptmather@syr.edu; Fax: +1 315-443-7724; Tel: +1 315-443-8760

† Electronic supplementary information (ESI) available: Example formulation; substrate characterization method; cell staining method; cell nuclear alignment analysis method; statistical analysis method; video of wrinkle formation; Differential Scanning Calorimetry (DSC) data; gold coating thickness analysis results; bulk shape recovery results; cell viability micrographs; and surface crack micrographs. See DOI: 10.1039/c3sm00024a

‡ Authors contributed equally to the work.

$$A = h_f\left(\frac{\varepsilon}{\varepsilon_c} - 1\right)^{\frac{1}{2}}$$

$$\varepsilon_c = \frac{1}{4}\left(\frac{3\bar{E}_s}{\bar{E}_f}\right)^{\frac{2}{3}}$$

here, $\bar{E} = E/(1 - \nu^2)$, ε_c is the critical or minimum strain that is necessary for buckling to occur, h_f is the film thickness, ν is Poisson's ratio, and $\bar{E}_f$ and $\bar{E}_s$ are the plane-strain moduli of the film and substrate, respectively.

While polydimethylsiloxane (PDMS) is the most popular compliant substrate used for wrinkle formation,[11,18,22,23,33] recent attention has turned to the use of shape memory polymers (SMPs) as "active" wrinkle substrates that can apply compression to a coating upon triggering a return from a temporarily strained state to the equilibrium, unstrained state.[34,35] The first reported use of an SMP as a substrate for wrinkle formation[36] involved a polystyrene SMP that yielded nano-scale, hierarchical wrinkles of a gold coating, and subsequent diversified approaches have included the IPH (Indentation–Polishing–Heating) process,[37] and the creation of localized structural colors.[38] Intended applications range from optical devices,[39] to electronics,[17,40,41] to controlled surface wettability[16,42] and biosensors.[36,43] Interested readers are referred to a recently published review article highlighting current work on wrinkle formation *via* the shape memory effect in polymers and metal alloys.[44]

In this work, our goal was to prepare a coated SMP bilayer system for the study of cell mechanobiology on previously wrinkled (static) and actively wrinkling (dynamic) substrates, recognizing the need to develop a "tunable" SMP that was compatible with cell culture. We hypothesized that by changing the amount of deformation fixed (and later recovered) in the new SMP substrate we could control the resulting wrinkle characteristics and the resulting degree of cellular alignment. In addition to studying cells cultured on previously wrinkled, static substrates, study of the response of cells to wrinkle formation during "active" cell culture is enabled for the first time. For active cell culture, cell seeding is performed at a cell-compatible temperature below body temperature and below the temperature at which wrinkles form, followed by a thermal activation at body temperature, forming wrinkles. In this manner, wrinkles form on a time scale comparable to both cell motility and cell division, yielding an opportunity to study dynamic interactions among the three phenomena.

Materials and methods

Substrate preparation

A copolymerization technique was employed to synthesize a substrate that can achieve wrinkle formation at 37 °C. Two monomers, *tert*-butyl acrylate (*t*BA) and butyl acrylate (BA), were mixed with a crosslinker, TEGDMA (triethylene glycol dimethacrylate), and a photoinitiator, DMPA (2,2-dimethoxy-2-phenyl acetophenone) [Scheme 1a], and injected between two glass slides with a 1 mm thick Teflon spacer. The monomers were passed through inhibitor removal columns (Scientific Polymer) prior to use, and the crosslinker and photoinitiator were used as received. Glass slides were treated with Rain-X to prevent adhesion with the cured SMP films. After injection, the mold was placed in a UV box (Black Ray, 365 nm, 2.0 mW cm^{-2}) featuring symmetric illumination from both sides of each specimen and allowed to cure for 1 h. The resulting polymer films were placed in methanol for 6 h for extraction and then dried in a vacuum oven at 55 °C overnight.

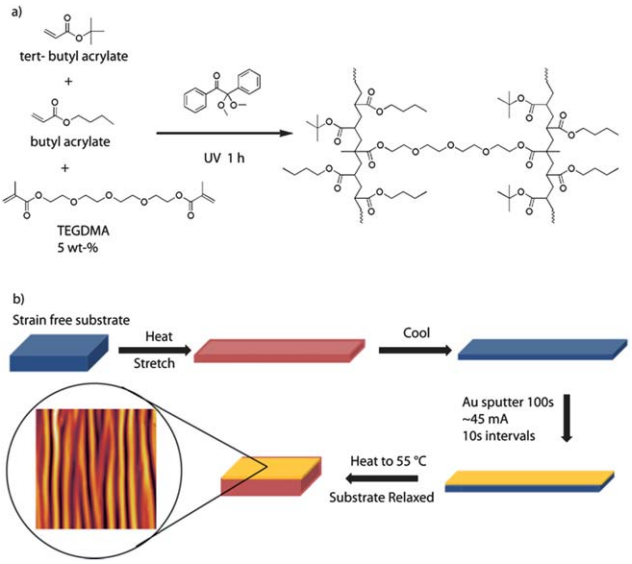

Scheme 1 Process for fabricating the wrinkled material. (a) Chemical structure of synthesized substrate, (b) stretching, coating, and recovering the substrate to form wrinkles.

The SMP glass transition temperature (T_g) was tuned by systematically varying the weight percentage of *t*BA and BA in the copolymer (Fig. S1†) while keeping the crosslinking density constant. By tuning the T_g of the system, control over the activation temperature for wrinkle formation could be achieved since the shape memory effect for amorphous-based SMPs is driven by the T_g. For each composition, the T_g was determined using differential scanning calorimetry (DSC) (TA Instruments Q200). The composition used further in this study was composed of 95 wt% *t*BA and 5 wt% BA, with a constant 5 wt% TEGDMA and 0.5 wt% DMPA, computed relative to the weight of co-monomers in the formulation (ESI Methods 1†).

Substrate characterization

Linear viscoelastic thermomechanical properties of the SMP substrate were determined using dynamic mechanical analysis (DMA) (TA Instruments Q800). A rectangular bar of the copolymer film was loaded in the tensile grips of the DMA at room temperature and sample linear viscoelastic properties at 1 Hz were measured as the temperature was ramped to 100 °C at a heating rate of 3 °C min^{-1} (ESI Methods 2†). Here, the strain-control mode of the instrument was utilized. To determine the shape memory characteristics of the SMP substrate, a

rectangular bar was first loaded in the DMA at room temperature. In controlled force mode, the sample was heated to 70 °C, deformed to 50% strain, and then cooled to 10 °C to fix the deformation through vitrification of the amorphous network chains. To recover the deformation, the sample was heated to 70 °C, completing the shape memory cycle. Three cycles were repeated to investigate shape memory reproducibility of the substrate. The fixing ratio (R_f), or the degree of fixing, and the recovery ratio (R_r) were calculated as:[45]

$$R_f(N) = \frac{\varepsilon_u(N)}{\varepsilon_m(N)} \times 100\%$$

$$R_r(N) = \frac{\varepsilon_u(N) - \varepsilon_p(N)}{\varepsilon_u(N) - \varepsilon_p(N-1)} \times 100\%$$

here N, ε_u, ε_m, and ε_p represent the cycle number, strain after unloading, strain before unloading, and the final strain after heating under no applied load, respectively.

To determine the thermomechanical properties of the substrate in the hydrated state, a rectangular bar of the sample was first equilibrated in water for 24 h. The sample was then loaded at room temperature into the DMA submersion clamp and heated to 70 °C at 2 °C min^{-1} while measuring the linear viscoelastic properties as a function of temperature at a frequency of 1 Hz. DSC was also performed on both dry and wet samples to determine T_g in order to compare with the DMA results.

Wrinkle formation

Wrinkle formation was enabled by compressive buckling of a gold coating that was first applied to an SMP that had been fixed with a temporary uniaxial strain and then recovered thermally. To fix a strain into the substrate, uniaxial stretching was conducted using the DMA. Samples were first heated to 80 °C and subsequently loaded until a prescribed strain was achieved. Upon reaching the prescribed strain the load was held constant and the samples were cooled to fix the prestrain into the substrate. Uniaxial prestrains of 2, 7, 12, 17, and 23% were investigated to ascertain the effect of prestrain on wrinkle characteristics. Next, a gold coating was applied to the substrate *via* sputtering. A total sputter time of 100 s was used to yield a 33 nm thick layer (Fig. S2†), measured using a method developed by Bowden *et al.*[11] Gold-coated substrates were placed in an isothermal oven at 55 °C for 30 min to allow the substrates to completely recover, resulting in wrinkle formation. In the water-triggered wrinkle formation experiment, the same sample preparation was conducted as described above; however, in these cases we examined wrinkle formation under conditions simulating those of cell culture. Thus, substrate recovery was performed in water at 30 °C for 5 h and then 24 h at 37 °C. A control experiment was conducted with a sample submerged in water for 5 h at 30 °C and then for an additional 24 h at 30 °C, which was expected not to yield wrinkles.

Wrinkle and crack characterization

Atomic force microscopy (AFM; Nano R-2 from Pacific Nanotechnology) with tapping mode was employed to characterize the resulting wrinkle morphologies. Two dimensional fast Fourier transforms (2D FFT) were performed to analyze the wrinkle wavelength distributions. The wavelength was calculated as the inverse of the wavenumber. A custom MATLAB program was written and used to calculate the wrinkle amplitude using AFM profiles. Wrinkle alignment analysis based on the 2D FFT images was conducted by ImageJ software using the "Oval plot" function. The full width at half maximum value was chosen to represent the relative degree of wrinkle alignment. Optical microscopy (OM) was utilized to image cracks that form during wrinkling and the crack density (CD) calculated as the inverse of the average crack spacing measured directly from the optical micrographs.

Cell culture

Prior to static and active cell culture experiments, human adipose derived stem cells (hASCs; Invitrogen) from a single donor were expanded in complete growth medium (MesenPro RS, 2% growth serum, 1% penicillin/streptomycin, 1% GlutaMAX). Cells were plated on T175 flasks at a seeding density of 5000 cells per cm^2 and expanded in a 37 °C humidified incubator with 5% CO_2. Growth medium was changed every 3 days and cells were passaged at 70% confluence using TrypLE. Cells at passages 6 and 7 were collected for the static and active cell experiments.

Cell culture on previously wrinkled substrates

To evaluate the extent to which cell alignment could be controlled by wrinkle properties, we seeded hASCs on substrates after wrinkle formation had occurred and quantified cell nuclear alignment (method details below). Following the procedure for wrinkle formation, SMPs with fixed uniaxial prestrains of 2, 7, 12, 17 and 23% were coated with gold and recovered for 2.5 h at 45 °C. A gold coated SMP with no prestrain was used as the control group. Samples from each group were cut into 6 mm × 6 mm squares and exposed to UV light for 10 h for sterilization. Samples were then equilibrated in complete medium for 5 h at room temperature to allow wetting of the surface. The samples were then placed in wells of a 48 well plate and seeded with a 20 μL droplet of cell solution at a concentration of 87 500 cells per mL. The plate was placed in a 37 °C incubator for 2 h to allow for cell attachment. After 2 h, 250 μL of additional medium was placed in each well and the plate was placed in a 37 °C incubator for an additional 22 h, after which point the cells were fixed and stained. For each group an n of 5 independent samples was used, where an independent sample was defined as being prepared from a separate cure of the SMP substrate.

Cell culture on actively wrinkling substrates

To investigate the effect of wrinkle formation on adherent-cell behavior, we plated hASCs on prestrained, gold-coated SMPs and analyzed cell behavior before and after triggering wrinkle formation. Prestrained, gold-coated samples were cut into 6 mm × 6 mm squares and exposed to UV light for 1 h for sterilization. Samples were equilibrated in complete medium at room

temperature for 5 h, after which they were placed in a 48 well plate and seeded with a 20 μL droplet of cell solution at a concentration of 87 500 cells per mL. The samples were placed in an incubator at 30 °C for 2 h to allow for cell attachment without triggering wrinkle formation. After 2 h, 250 μL of additional medium pre-warmed to 30 °C was added to each well and the plate was placed in a 30 °C incubator for 3 h to allow cells to spread. After 3 h, cells on one set of samples were fixed, stained, and imaged to determine cell alignment before wrinkle formation. A second set of samples was left in the 30 °C incubator for an additional 24 h to serve as the control, and the third set, the experimental group, was placed in a 37 °C incubator for an additional 24 h, triggering wrinkle formation. These groups were fixed, stained, and imaged to evaluate cell alignment. For each group an n of 5 independent samples was used.

Cell staining and imaging

Both the cell nucleus and the actin cytoskeleton were stained to quantitatively and qualitatively assess cell alignment. Alexa Fluor 647 conjugated phalloidin (Invitrogen) was used to stain the actin cytoskeleton, and DAPI was used to stain the nucleus (ESI Methods 3†). Cells stained with phalloidin and DAPI were imaged using a Leica DMI 4000B inverted microscope. Images were captured with a Leica DFC 340FX camera using a 10×/0.22 NA objective. Pseudocolor was applied to the micrographs using Leica Application Suites software, and histogram stretching was used to increase contrast for the images.

Cell nuclear alignment determination

To quantify cell alignment of DAPI-stained samples, the nuclear angle for each cell was determined using ImageJ (ESI Methods 4†), and the standard deviation of the angular distribution was determined. The standard deviation was used to determine the degree of orientation, as it has been shown to be a simple means of determining degree of alignment:[46] randomly distributed nuclear angles would produce a standard deviation of 52°, whereas perfectly aligned nuclear angles would produce a standard deviation of 0°.

Statistics

One factor ANOVA was performed to test for significant differences between the standard deviation of nuclear angle for any group. Permutation testing was then used for multiple comparison tests. Statistical significance was set at the $P < 0.05$ level.

Results

Substrate material properties

We designed a copolymer network with a tunable T_g to serve as an active substrate in our coated SMP bilayer system. A copolymer composition of 95 wt% *t*BA and 5 wt% BA yielded a T_g of 45 °C (dry), which is lowered to 40 °C (Fig. S3†) once hydrated due to water plasticization. As shown in Fig. 1a, the copolymer was subjected to three subsequent one-way shape memory cycles, revealing excellent shape fixing and recovery properties with values greater than 97% for each. This copolymer also showed excellent reproducibility, as there was no detectable loss in fixing or recovery between the three consecutive shape memory cycles. As expected, the tensile storage modulus dropped dramatically near T_g for both dry and water-saturated samples (Fig. 1b). Since our system is a T_g-based shape memory polymer, we reason that absorption served to plasticize the polymer matrix, causing a slight decrease in T_g. For this system the plasticization lowered the T_g by 3–5 °C which agreed with the DSC results (Fig. S3†). Indeed, this is why the T_g of the substrate in the dry state was designed to slightly exceed 37 °C.

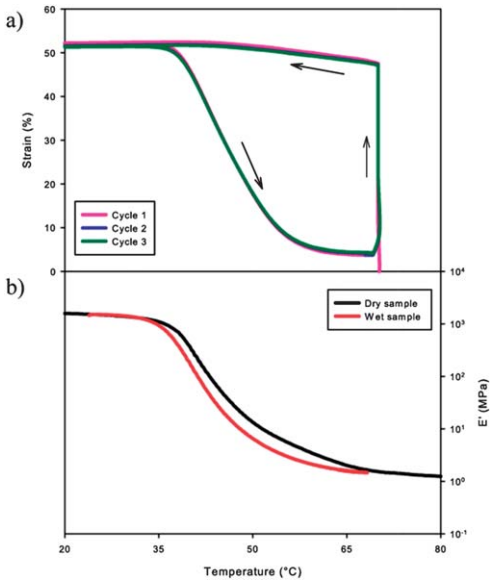

Fig. 1 Thermomechanical properties of the *t*BA/BA substrate. (a) Shape memory cycle and (b) effect of temperature on tensile storage modulus for dry and hydrated samples.

Strain effect on wrinkle–crack properties

Wrinkles formed by recovery of prestrains ranging from 2% to 23% were investigated to reveal any strain-dependence on wrinkle characteristics. From the AFM scans (Fig. 2, left) it is qualitatively clear that increasing prestrain tends to increase wrinkle amplitude, while the wrinkle wavelength decreases. This effect was further supported by the 2D FFT analysis which showed a shift of the entire wrinkle wavelength distribution toward smaller wavelengths (larger wavenumber) with increasing prestrain (Fig. 3). The wrinkle wavelength was found to decrease with prestrain (Fig. 4a), whereas the wrinkle amplitude appeared to increase with prestrain (Fig. 4b). It was also found that increasing prestrain led to the appearance of two or more characteristic wrinkle wavelength peaks in response to substrate recovery. Qualitative inspection of 2D FFT azimuthal scans (Fig. 3c) suggests that the degree of alignment is similar for all wrinkled samples, independent of prestrain. Quantitatively, however, the full-width-at-half-maximum plots of the same datasets (Fig. 4c) reveal that orientation increased with increasing prestrain. Cracks (Fig. 2, right) showed a strong

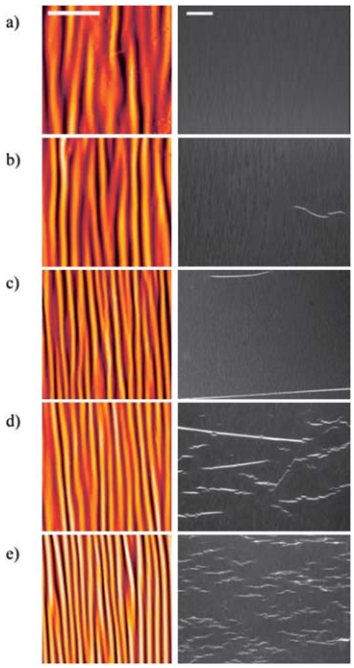

Fig. 2 AFM wrinkle images (left) and OM crack images (right) with prestrain values of (a) 2%, (b) 7%, (c) 12%, (d) 17%, and (e) 23%. Heights in AFM images are given in color scale and range from $z = 0$ nm black pixels to $z = 700$ nm bright pixels. Scale bar is 20 μm for AFM image (left) and 200 μm for OM image (right).

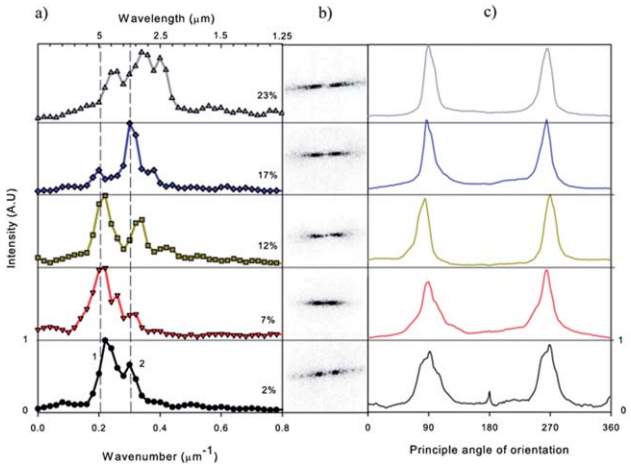

Fig. 3 Characterization of wrinkles using 2D FFT. (a) Wavelength distributions of uniaxial wrinkles with a controlled thickness of gold and varying prestrain, (b) 2D FFT pattern of wrinkled surfaces, (c) relative degree of alignment characterization using 2D FFT pattern. "1" and "2" in the left frame indicate the first and second populations of uniaxial wrinkle wavelengths.

dependence on prestrain. In particular, cracks formed for prestrains larger than 7%, beyond which crack density increased with prestrain. (Note: Fig. 4d is discussed below.)

Wrinkle formation in simulated cell-culture conditions

Wrinkle formation in the hydrated state – here termed "active wrinkling" – was investigated to determine whether or not our bilayer system was stable at 30 °C (cell seeding temperature) and whether or not it would fully recover at 37 °C (activation

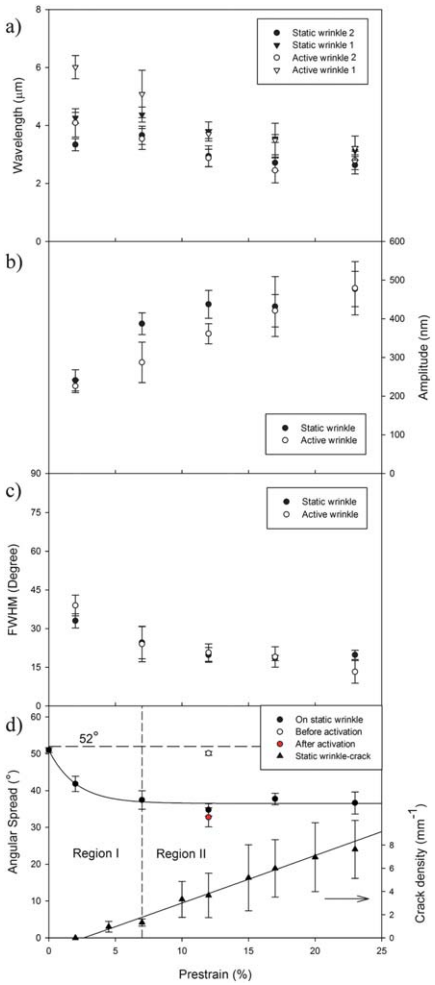

Fig. 4 Characterization of static wrinkles and active wrinkles. (a) Wavelength change with respect to the prestrain, (b) amplitude dependence on wrinkle prestrain, (c) relative degree of alignment as a function of prestrain. (d) Cell orientation with respect to wrinkle prestrain. The controlled gold thickness in (a)–(d) is 33 nm. "1" and "2" in (a) indicate the first and second populations of uniaxial wrinkle wavelengths.

temperature for active cell experiment). Gratifyingly, we observed no wrinkle formation in water at room temperature and 30 °C for 5 h (Fig. 5) but wrinkles formed when the water temperature was elevated to 37 °C, which was expected, as the SMP substrate demonstrates bulk recovery at 37 °C when hydrated (Fig. S4†). Wrinkles formed in the wet state were compared to wrinkles formed in the dry state. Wavelengths ranging from 2 to 6 μm, comparable to those observed in the dry state, were observed for the water-triggered wrinkle experiment using 2D FFT analysis (Fig. 4). Notably, the wrinkle amplitude began to saturate at the highest prestrains examined. No significant differences in wrinkle alignment and amplitude were observed when comparing wrinkles formed under dry (static in cell culture) and wet (active in cell culture) conditions (Fig. 4b and c).

Cell culture on previously wrinkled substrates

We compared cell alignment on wrinkled samples prepared from prestrains of 2, 7, 12, 17, and 23% to cell alignment on a

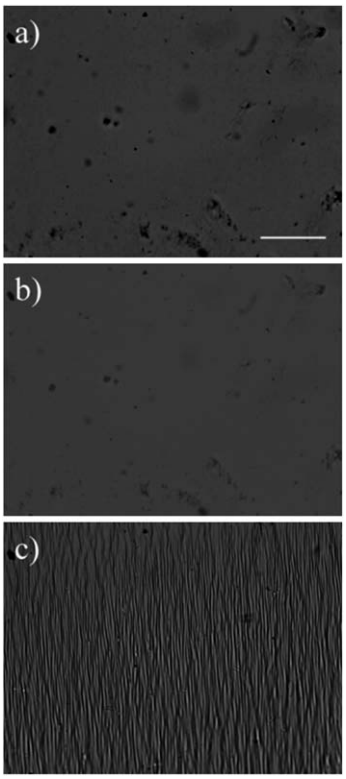

Fig. 5 Optical micrographs of water triggered wrinkle formation with a 100 s gold coating and 12% prestrain. (a) In water at 30 °C for 5 h. (b) In water at 30 °C for 29 h. (c) In water at 30 °C for 5 h followed by 37 °C for an additional 24 h. The scale bar is 50 μm and applies to all three images.

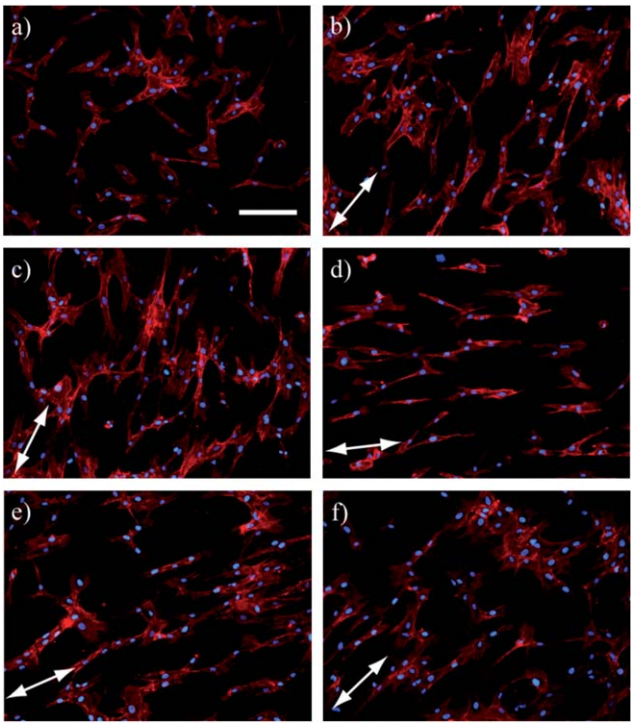

Fig. 6 Wrinkle effect on cell alignment. Phalloidin (cytoskeleton) and DAPI (nuclear) assays performed on cells seeded on (a) non-wrinkled, (b) 2%, (c) 7%, (d) 12%, (e) 17%, and (f) 23% prestrain. Scale bar is 200 μm. Cytoskeleton stain is shown in red and nuclear stain in blue. Cells on the non-wrinkled sample appear randomly distributed whereas cells on all wrinkled samples show alignment parallel to the wrinkle direction.

non-wrinkled sample by staining and imaging cell nuclei and f-actin 24 h after seeding. We note that cells for all groups showed high viability (Fig. S5†). On the non-wrinkled substrate (Fig. 6a), the cell cytoskeleton appears spread and elongated in all directions, showing no preferential angle of orientation. However, on wrinkled substrates of all prestrains (Fig. 6b–f), the cell cytoskeleton appears spread and elongated parallel to the wrinkle direction.

The degree of cell alignment was quantified by fitting ellipses to cell nuclei and calculating the standard deviation of the resulting cell nuclear angles. A large distribution of nuclear angles was found on the non-wrinkled sample (Fig. 6a), whereas a narrow distribution of nuclear angles was found on all wrinkled samples (Fig. 6b–f). For each angular histogram, the wrinkle direction was chosen as a reference orientation set at 90°.

For the wrinkled samples, each distribution is centered about this angle, demonstrating that the preferential angle of orientation is parallel to the wrinkle direction. The resulting standard deviation of the nuclear angles was calculated for each group and plotted as a function of prestrain (Fig. 4d). For the non-wrinkled sample (0% prestrain), a standard deviation of $51.0 \pm 0.7°$ was found, consistent with a random distribution of nuclear angles. As the prestrain increased, the resulting angular standard deviation decreased until saturating beyond 7% prestrain. Comparing this trend to the trends of wrinkle amplitude and wavelength with increasing prestrain (Fig. 4a and b), we find significant correlation but are unable to determine which wrinkle characteristic dictates nuclear alignment. Correlation of cell alignment to the wrinkle aspect ratio, determined as amplitude divided by wavelength, was also investigated but no clear conclusion could be drawn (Fig. S9†). Noticeably, crack density (Fig. 4d) showed a gradual and nearly linear increase with prestrain that apparently saturates wrinkle refinement with strain and thus saturates the degree of cell alignment. Inspection of Fig. 4d reveals roughly four regions of behaviour. In region I, where prestrain is lower than 7%, cell nuclear alignment increased with increasing prestrain as shown by a decrease in angular spread. Meanwhile, cracks were observed with prestrain larger than 4.5%. In region II, where prestrain is higher than 7%, cell nuclear orientation plateaued while crack density increased. Thus, increasing SMP prestrain increases the degree of nuclear orientation, a phenomenon that offers quite interesting potential for future studies, but methods that suppress crack formation may be needed to extend the control of nuclear alignment to higher extents.

Cell culture on actively wrinkling substrates

Cellular response to actively wrinkling substrates was assessed by imaging cell nuclei and f-actin first on cells cultured on a wrinkle-free, prestrained (and coated) substrate at a sub-trigger temperature ($T = 30$ °C) and then at a higher temperature ($T = 37$ °C) capable of triggering wrinkle formation. We observed no obvious cytoskeleton orientation prior to wrinkle formation (Fig. 7a);

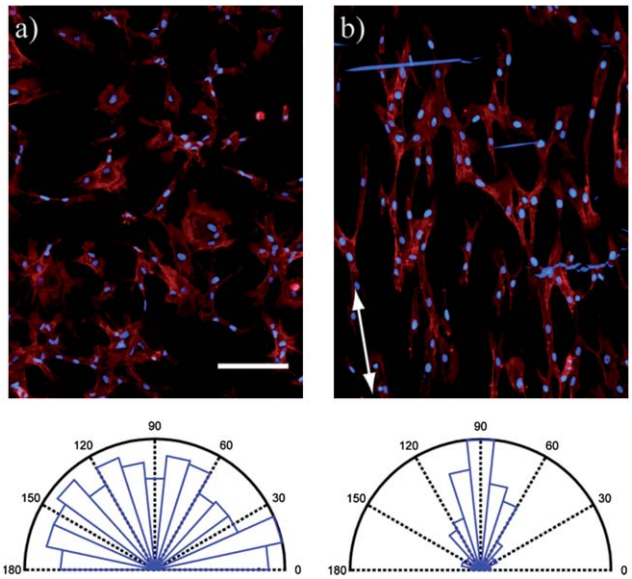

Fig. 7 Cell morphology before (a) and after (b) wrinkling. Phalloidin (cytoskeleton) and DAPI (nuclear) assays were performed on cells seeded (a) at 30 °C for 5 h and (b) at 30 °C for 5 h followed by 37 °C for 24 h. Scale bar is 200 μm. Cells show no orientation prior to wrinkle formation and subsequently align parallel to the wrinkle direction after wrinkle formation is triggered. Angular histograms show the distribution of cell nuclear angles, with a broad distribution of angles representing no alignment and a narrow distribution representing a high degree of alignment. The 90° angle in the angular histogram represents the angle parallel to the wrinkles.

however, as a result of wrinkle formation the cytoskeleton elongated parallel to the wrinkle direction (Fig. 7b). Similar results were found for cell nuclear orientation, assessed by fitting ellipses to cell nuclei and determining the spread of nuclear angles, as was done described above for cells cultured on previously wrinkled substrates. Interestingly, while a broad distribution of nuclear angles was observed before wrinkling (Fig. 7, histogram beneath (a)), this distribution significantly narrowed upon wrinkle formation (Fig. 7, histogram beneath (b)). Comparison of the two types of experiments (cellular response to previously wrinkled *versus* actively wrinkling substrates) is seen in Fig. 4d. In the latter case, an average angular standard deviation of 50.1 ± 0.5° was found prior to triggering, whereas an average angular standard deviation of 32.7 ± 2.5° was found after triggering wrinkle formation – close to the value for nuclear alignment of cells cultured on previously wrinkled substrates (34.8 ± 1.7°). A control group of cells left at 30 °C for the 24 h after seeding showed no preferential orientation (Fig. S6†). Cells in all cases showed high viability (Fig. S7†).

Discussion

In this study we demonstrated a coated SMP bilayer system capable of forming tunable wrinkles under conditions amenable to cell culture, namely, in aqueous media at temperatures near and including 37 °C. More importantly, cell culture on both previously wrinkled and actively wrinkling substrates was proven to result in clear orientation of both f-actin and ellipsoidal cell nuclei. Prior to wrinkle formation, no preferential angle of orientation was observed; however, as a result of wrinkle formation whose amplitude increased and wavelength decreased with increasing recovered strain, clear cell orientation was observed with orientation along the wrinkle direction and with a degree that increased with wrinkle amplitude.

Considering wrinkle formation results alone, we observed that our bilayer wrinkle system agreed well with the prestrain dependence for both wavelength and amplitude described by Jiang *et al.*[47] In contrast, a report by Xie *et al.* showed that while wrinkle wavelength decreased with increasing recovered strain, no dependence of amplitude on strain was observed.[38] We are currently unable to explain the difference between this result and our results reported in Fig. 4. A salient feature of the SMP-triggered wrinkles reported in Fig. 3 is the broad distribution of wrinkle wavelengths observed. Such hierarchical wrinkling has been reported before and found to be associated with large compressive stress.[18] It is understood that the origin of this phenomenon is the saturation of first generation wrinkles at a small amplitude which forms an effective film that can undergo a similar wrinkling process. This hierarchical buckled pattern forms with further application of a compressive strain. However, the mechanism for our bilayer wrinkle system is different. Heating the SMP above its glass transition temperature induces the transition from the glassy to the rubbery state during which the modulus decreases several orders of magnitude. In particular, while the surface buckling process at lower temperatures favours smaller wavelengths, larger wavelengths are favoured at higher temperatures. Thus, the evolving modulus change with continued increase in temperature during heat-triggered shape-recovery resulted in a distribution of wrinkle wavelengths. Further, while the linear buckling theory[29,30] has proven to work well for elastic substrates, our system is viscoelastic[48–50] and thus features significant time-dependence that we are currently exploring. Using linear theory, we did a simple calculation to compare our results to the predicted theoretical values with the following parameters. For gold (f) and the SMP substrate (s), E_f = 82 GPa, ν_f = 0.33, E_s (dry 55 °C) = 5 MPa. E_s (wet 37 °C in Fig. S10†) = 515 MPa, ν_s = 0.44 (assumed). In the case where wrinkles were formed under dry conditions, the predicted wavelength is 3.5 μm, which is in the range of our experimental result. However, for wrinkles formed in water at 37 °C, the predicted wavelength is 0.75 μm, at least 4 times lower than our experimental value. We are currently unable to explain this discrepancy, but tentatively point to a viscoelastic effect. Clearly, an SMP wrinkle model will need to be developed in the future.

Cracks (Fig. 2) were also observed to form for samples that were prestrained 7% and higher, with an increase in crack density with increasing prestrain (Fig. 2 and 4). By comparison, the crack spacing is much larger than the wrinkle wavelength for all conditions explored. We attribute the formation of cracks to the SMP's lateral elongation[13] that occurs during recovery, which induces a tensile stress in the gold in the direction perpendicular to the direction of recovery. Interestingly, the onset prestrain of crack formation corresponded to the beginning of saturation in both wrinkle characteristics and degree of

cell alignment (Fig. 4). The crack density data in Fig. 4d were fitted into a power-law function[52]

$$\mathrm{CD} = c(\varepsilon - \varepsilon^*)^{\beta}$$

where c is a constant, ε^* is the critical strain for cracking, and β is an exponent governing the rate of fragmentation. Our fitting equation yielded an ε^* of 2.6% and $\beta \sim 1.0$. For still higher strains, it is likely that the fragmentation process will also saturate to yield $\beta < 1$.

We observed without exception that the wrinkles formed on our SMP, whether before or during cell culture, remained in apparently unadulterated form following prolonged exposure to cell culture conditions. Gratifyingly, we did not observe delamination between the gold coating and SMP substrate, neither during wrinkle formation nor cell culture. This suggests a robust interface despite not using an adhesion interlayer that is sometimes required.[11,53,54] However, an additional interlayer such as titanium (Ti) could improve the adhesion and further suppress crack formation when submerged in medium for longer culture periods. Nano-sized gold coatings are known to be plastic with a very low yield strain. The strain applied on the gold from the substrate was irreversible and the gold thickness could have potentially changed due to plastic deformation. Whether the gold thickness and stiffness were changed during wrinkling is still unknown. Further studies can be conducted to investigate the effect of this mechanical loading on the thin gold film properties. For the present study, we focused on cell behaviour far from cracks; however, the interaction of cells with cracks may be an interesting area for future study due to large tensile strains that could be applied to cells spanning a crack. To clarify the role of wrinkle wavelength distribution, we must first learn how to control this distribution width, average wavelength, and amplitude independently, an endeavour of great interest to us.

While the complex topography associated with hierarchical wrinkles is thought useful for microfluidic sieves,[18] antifouling marine coatings,[51] and substrates for cell mechanosensitivity studies,[21] its relevance, *per se*, to cell culture substrates has not yet been revealed. Here, we were able to control the degree of cell alignment by variation in wrinkle characteristics. By increasing the prestrain in the SMP we were able to increase the degree of wrinkle orientation as well as increase the wrinkle amplitude. This resulted in increasing degrees of cell alignment until saturation occurred after 7% prestrain. The increase in cell alignment can be attributed to both the increase in orientation of the wrinkles and the increase in wrinkle amplitude. Which of these two is the prominent cause is unknown, and further studies would need to be conducted to isolate each effect and determine which played a more significant role. Prior studies have found that atop grating patterns cell alignment increases with grating depth.[5,6,55] Cell alignment (Fig. 4d) showed an exponential decay that followed the following form:

$$y = 36.49 + 14.48\mathrm{e}^{-0.494x}$$

where x is the prestrain (%) and y is the angular spread of nuclear orientation in degrees. The saturation of cell alignment at prestrains above 7% is strongly correlated with the onset of crack density growth as noted above. This dynamic approach also proved to be a viable way of turning on cell alignment. Prior to topography change, cells had shown a random orientation, whereas shortly after activating the topography change cells re-oriented parallel to the wrinkle direction. This effect was observed previously in the work by Lam *et al.*, who used an external force to compress a PDMS substrate that had a thin oxidized film resting atop, forming wrinkles while cells were attached.[56] Our system expands on the work by Lam and colleagues because here we have a material intrinsically capable of forming wrinkles in culture without the need for an external compression mechanism and with the potential for control over the time scale of their formation.

The present work contributes to recent progress in SMPs designed for application in cell culture. Neuss and colleagues reported use of a polycaprolactone dimethacrylate polymer substrate that was uniaxially stretched and fixed prior to cell seeding. The sample was triggered to recover at a temperature of 54 °C, and apoptotic cells were observed after activation due to this hyperthermic transition temperature.[57] We recently overcame this obstacle by synthesizing an SMP with a trigger temperature near 37 °C, allowing for cells to be viable both during and after activation. We found that, at the micro-scale, shape-memory activated changes in substrate topography could direct cell orientation.[58] Subsequently, Sheares Ashby and colleagues reported similar cell alignment findings using a polycaprolactone SMP with smaller feature sizes and a hyperthermic trigger temperature of 41 °C.[59] Here we have shown that a wrinkled topography can be controlled simply by changing the prestrain in the SMP, and with this system we are able to trigger wrinkle formation at 37 °C. It is important to note that the cell alignment observed on the actively wrinkling substrate was similar to that observed on its previously wrinkled counterpart. Further studies into the dynamics of cell alignment through time-lapse microscopy may reveal transient cell alignment during active wrinkling that may differ from the equilibrium state. Also of interest to our group is the effect of wrinkling kinetics on cell behaviour, recognizing the possibility of distinct regimes for strain rates[60,61] applied to adherent cells.

One advantage of this system is that the composition can be tuned to obtain a range of T_g's, which can be used to study how the dynamics of topography change elicit different effects from cells. This extension of the present work should improve our fundamental understanding of the mechanisms behind cell–material interactions in a dynamic state. Studies employing actively changing topography on a time scale slower than, similar to, or faster than that of cell cytoskeleton reorganization will provide unprecedented new insight into cell cytoskeleton reorganization and cell mechanobiology.

Conclusions

We have developed a biocompatible coated SMP bilayer system with tunable wrinkle formation that can be used to direct cell alignment in static and active culture experiments. An increase in prestrain of the SMP led to an increase in wrinkle amplitude

and orientation and a decrease in wrinkle wavelength. Subsequently, the degree of cell alignment in static cultures increased with increasing SMP prestrain until saturation occurred. Furthermore, this system showed that cell alignment can be turned on through triggering wrinkle formation during active cell culture. The ease of which the transition temperature of this system can be tuned should enable the study of the kinetic effects of topography change on cellular response.

Acknowledgements

This material is based upon work supported by a grant awarded to JHH and PTM: NSF Grant no. DMR-0907578.

Notes and references

1 D. E. Ingber, *Circ. Res.*, 2002, **91**, 877–887.
2 M. A. Wozniak and C. S. Chen, *Nat. Rev. Mol. Cell Biol.*, 2009, **10**, 34–43.
3 S. Suresh, *Acta Biomater.*, 2007, **3**, 413–438.
4 S. R. Bhattarai, N. Bhattarai, H. K. Yi, P. H. Hwang, D. I. Cha and H. Y. Kim, *Biomaterials*, 2004, **25**, 2595–2602.
5 A. I. Teixeira, P. F. Nealey and C. J. Murphy, *J. Biomed. Mater. Res., Part A*, 2004, **71**, 369–376.
6 W. Hu, E. K. F. Yim, R. M. Reano, K. W. Leong and S. W. Pang, *J. Vac. Sci. Technol., B: Microelectron. Nanometer Struct.–Process., Meas., Phenom.*, 2005, **23**, 2984–2989.
7 A. S. G. Curtis, B. Casey, J. O. Gallagher, D. Pasqui, M. A. Wood and C. D. W. Wilkinson, *Biophys. Chem.*, 2001, **94**, 275–283.
8 C. C. Berry, G. Campbell, A. Spadiccino, M. Robertson and A. S. G. Curtis, *Biomaterials*, 2004, **25**, 5781–5788.
9 M. J. Dalby, N. Gadegaard, R. Tare, A. Andar, M. O. Riehle, P. Herzyk, C. D. W. Wilkinson and R. O. C. Oreffo, *Nat. Mater.*, 2007, **6**, 997–1003.
10 C. J. Bettinger, R. Langer and J. T. Borenstein, *Angew. Chem., Int. Ed.*, 2009, **48**, 5406–5415.
11 N. Bowden, S. Brittain, A. G. Evans, J. W. Hutchinson and G. M. Whitesides, *Nature*, 1998, **393**, 146–149.
12 W. T. S. Huck, N. Bowden, P. Onck, T. Pardoen, J. W. Hutchinson and G. M. Whitesides, *Langmuir*, 2000, **16**, 3497–3501.
13 A. L. Volynskii, S. Bazhenov, O. V. Lebedeva and N. F. Bakeev, *J. Mater. Sci.*, 2000, **35**, 547–554.
14 S. J. DuPont, R. S. Cates, P. G. Stroot and R. Toomey, *Soft Matter*, 2010, **6**, 3876–3882.
15 T. Tanaka, S. T. Sun, Y. Hirokawa, S. Katayama, J. Kucera, Y. Hirose and T. Amiya, *Nature*, 1987, **325**, 796–798.
16 S. Yang, K. Khare and P. C. Lin, *Adv. Funct. Mater.*, 2010, **20**, 2550–2564.
17 D. Y. Khang, J. A. Rogers and H. H. Lee, *Adv. Funct. Mater.*, 2009, **19**, 1526–1536.
18 K. Efimenko, M. Rackaitis, E. Manias, A. Vaziri, L. Mahadevan and J. Genzer, *Nat. Mater.*, 2005, **4**, 293–297.
19 M. W. Moon and A. Vaziri, *Scr. Mater.*, 2009, **60**, 44–47.
20 M. Wang, J. E. Comrie, Y. P. Bai, X. M. He, S. Y. Guo and W. T. S. Huck, *Adv. Funct. Mater.*, 2009, **19**, 2236–2243.
21 H. Vandeparre, S. Gabriele, F. Brau, C. Gay, K. K. Parker and P. Damman, *Soft Matter*, 2010, **6**, 5751–5756.
22 D. C. Hyun and U. Jeong, *J. Appl. Polym. Sci.*, 2009, **112**, 2683–2690.
23 P. C. Lin and S. Yang, *Appl. Phys. Lett.*, 2007, **90**, 241903.
24 A. Chiche, C. M. Stafford and J. T. Cabral, *Soft Matter*, 2008, **4**, 2360–2364.
25 X. Chen and J. W. Hutchinson, *J. Appl. Mech.-Trans. ASME*, 2004, **71**, 597–603.
26 C. Jiang, S. Singamaneni, E. Merrick and V. V. Tsukruk, *Nano Lett.*, 2006, **6**, 2254–2259.
27 M. Guvendiren, J. A. Burdick and S. Yang, *Soft Matter*, 2010, **6**, 5795–5801.
28 M. Guvendiren and J. A. Burdick, *Biomaterials*, 2010, **31**, 6511–6518.
29 J. Y. Chung, A. J. Nolte and C. M. Stafford, *Adv. Mater.*, 2011, **23**, 349–368.
30 R. Huang and Z. Suo, *J. Appl. Phys.*, 2002, **91**, 1135–1142.
31 J. Song, H. Jiang, Z. J. Liu, D. Y. Khang, Y. Huang, J. A. Rogers, C. Lu and C. G. Koh, *Int. J. Solids Struct.*, 2008, **45**, 3107–3121.
32 J. Y. Chung, T. Q. Chastek, M. J. Fasolka, H. W. Ro and C. M. Stafford, *ACS Nano*, 2009, **3**, 844–852.
33 C. Bukowsky, J. M. Torres and B. D. Vogt, *J. Colloid Interface Sci.*, 2011, **354**, 825–831.
34 P. T. Mather, X. F. Luo and I. A. Rousseau, *Annu. Rev. Mater. Res.*, 2009, **39**, 445–471.
35 M. Behl, M. Y. Razzaq and A. Lendlein, *Adv. Mater.*, 2010, **22**, 3388–3410.
36 C. C. Fu, A. Grimes, M. Long, C. G. L. Ferri, B. D. Rich, S. Ghosh, L. P. Lee, A. Gopinathan and M. Khine, *Adv. Mater.*, 2009, **21**, 4472–4476.
37 L. Sun, Y. Zhao, W. M. Huang and T. H. Tong, *Surf. Rev. Lett.*, 2009, **16**, 929–933.
38 T. Xie, X. C. Xiao, J. J. Li and R. M. Wang, *Adv. Mater.*, 2010, **22**, 4390–4394.
39 R. M. Braun and R. Sharma, Silicone contact lenses with wrinkled surface, *US Pat.* 20 080 206 481, 2008.
40 D. Y. Khang, H. Q. Jiang, Y. Huang and J. A. Rogers, *Science*, 2006, **311**, 208–212.
41 Y. G. Sun, W. M. Choi, H. Q. Jiang, Y. G. Y. Huang and J. A. Rogers, *Nat. Nanotechnol.*, 2006, **1**, 201–207.
42 J. Y. Chung, J. P. Youngblood and C. M. Stafford, *Soft Matter*, 2007, **3**, 1163–1169.
43 L. Zhang, X. Y. Lang, A. Hirata and M. W. Chen, *ACS Nano*, 2011, **5**, 4407–4413.
44 L. Sun, Y. Zhao, W. M. Huang, H. Purnawali and Y. Q. Fu, *Surf. Rev. Lett.*, 2012, **19**, 1250010.
45 X. F. Luo and P. T. Mather, *Macromolecules*, 2009, **42**, 7251–7253.
46 P. Davidson, M. Bigerelle, B. Bounichane, M. Giazzon and K. Anselme, *Acta Biomater.*, 2010, **6**, 2590–2598.
47 H. Q. Jiang, D. Y. Khang, J. Z. Song, Y. G. Sun, Y. G. Huang and J. A. Rogers, *Proc. Natl. Acad. Sci. U. S. A.*, 2007, **104**, 15607–15612.

48 P. J. Yoo and H. H. Lee, *Macromolecules*, 2005, **38**, 2820–2831.
49 E. P. Chan, S. Kundu, Q. H. Lin and C. M. Stafford, *ACS Appl. Mater. Interfaces*, 2011, **3**, 331–338.
50 P. J. Yoo and H. H. Lee, *Phys. Rev. Lett.*, 2003, **91**, 154502.
51 K. Efimenko, J. Finlay, M. E. Callow, J. A. Callow and J. Genzer, *ACS Appl. Mater. Interfaces*, 2009, **1**, 1031–1040.
52 J. Y. Chung, J. H. Lee, K. L. Beers and C. M. Stafford, *Nano Lett.*, 2011, **11**, 3361–3365.
53 A. L. Volynskii, D. A. Panchuk, S. V. Moiseeva, A. S. Kechek'yan, A. I. Dement'ev, L. M. Yarysheva and N. F. Bakeev, *Russ. Chem. Bull.*, 2009, **58**, 865–882.
54 D. C. Hurley, M. Kopycinska-Muller, E. D. Langlois, A. B. Kos and N. Barbosa, *Appl. Phys. Lett.*, 2006, **89**, 021911.
55 J. R. Sun, Y. F. Ding, N. J. Lin, J. Zhou, H. Ro, C. L. Soles, M. T. Cicerone and S. Lin-Gibson, *Biomacromolecules*, 2010, **11**, 3067–3072.
56 M. T. Lam, W. C. Clem and S. Takayama, *Biomaterials*, 2008, **29**, 1705–1712.
57 S. Neuss, I. Blomenkamp, R. Stainforth, D. Boltersdorf, M. Jansen, N. Butz, A. Perez-Bouza and R. Knuchel, *Biomaterials*, 2009, **30**, 1697–1705.
58 K. A. Davis, K. A. Burke, P. T. Mather and J. H. Henderson, *Biomaterials*, 2011, **32**, 2285–2293.
59 D. M. Le, K. Kulangara, A. F. Adler, K. W. Leong and V. S. Ashby, *Adv. Mater.*, 2011, **23**, 3278–3283.
60 B. D. Hoffman and J. C. Crocker, *Annu. Rev. Biomed. Eng.*, 2009, **11**, 259–288.
61 P. A. Janmey and C. A. McCulloch, *Annu. Rev. Biomed. Eng.*, 2007, **9**, 1–34.

